Check for updates

Can Hydrated Electrons be Produced from Water with Visible Light?

Sebastian Pios,[a] Xiang Huang,[a] and Wolfgang Domcke*[a]

Ab initio computational methods are employed to explore whether hydrated electrons can be produced by the photodetachment of the excess hydrogen atom of the heptazinyl radical (HzH) in finite-size HzH⋯$(H_2O)_n$ clusters. The HzH radical is an intermediate species in the photocatalytic oxidation of water with the heptazine (Hz) chromophore. Hz (heptaazaphenalene) is the monomer of the ubiquitous polymeric water-oxidation photocatalyst graphitic carbon nitride (g-C_3N_4). The energy profiles of minimum-energy excited-state reaction paths for proton-coupled electron transfer from HzH to water molecules were computed for the HzH⋯H_2O and HzH⋯$(H_2O)_4$ complexes with the CASPT2 method. The results reveal that the photodetachment of the excess H-atom from the HzH radical is a barrierless reaction in these hydrogen-bonded complexes, resulting in the formation of H_3O and $H_3O(H_2O)_3$ radicals, respectively, which are finite-size models of the hydrated electron. The computational results suggest that the photocatalytic formation of hydrated electrons from water with visible light could be possible in principle.

1. Introduction

The hydrated electron is a metastable defect in liquid water which is readily generated with ionizing radiation.[1–6] The hydrated electron is defined by its characteristic intense and broad absorption spectrum peaking at 720 nm.[1] The defect has a lifetime of about 1 μs in ultrapure water at room temperature.[2] The hydrated electron is a species with one of the highest reduction potentials in chemistry.[3] While the properties and the reactivity of the hydrated electron were extensively investigated since decades,[2,3] the structure of this defect of liquid water at the atomic level is still a matter of considerable debate.[7–14] The main-stream opinion favours the so-called cavity model, that is, a localized electron cloud confined in a cavity of the hydrogen-bonded network of water.[5–7,12,15,16] Alternative models with more molecular flavour, such as H_3O–OH^- complexes, were proposed early by Robinson and co-workers[17] and Tuttle and Golden.[18] The hydrated hydronium, H_3O–$(H_2O)_n$, model of the solvated electron is supported by more recent ab initio calculations for finite-size clusters.[19,20] It has been shown that hydrated H_3O radicals exhibit absorption spectra which converge rapidly with increasing cluster size toward the characteristic absorption spectrum of the hydrated electron in liquid water.[19] Moreover, these radicals undergo spontaneous charge separation, forming a

hydronium cation (H_3O^+) loosely bonded with a solvated electron cloud.[19,20] The hydrated hydronium model for finite clusters and the standard cavity model for bulk water therefore are not fundamentally different.[6] Recent investigations of hydrated electron formation by XUV-induced radiolysis in large water clusters by time-resolved photoelectron imaging provided strong evidence that the primary step of the radiolysis is hydrogen-atom transfer, resulting in the formation of hydrated hydronium radicals which subsequently separate into hydrated hydronium cations and presolvated electrons.[21]

The hydrated electron can also be produced by photodetachment from solvated anions,[22] such as I^-, or by photoexcitation of certain aromatic chromophores, so-called photoacids, e.g. phenol, indole or DNA bases.[23–27] Recently, it has been shown that hydrated electrons also can be ejected by UV irradiation from diamond substrates into water[28] and it has been found that these hydrated electrons can selectively reduce carbon dioxide to carbon monoxide[29,30] and molecular nitrogen to ammonia[31–33] in the aqueous phase. These findings suggest that the exceptionally high reduction potential of the hydrated electron could possibly be exploited to achieve the transformation of abundantly available feedstock chemicals (CO_2, N_2) to renewable fuels (e.g. methanol or ammonia) if the hydrated electron could efficiently and sustainably be produced with sunlight rather than with UV radiation.

The sustainable production of hydrated electrons requires that the electrons are obtained by photooxidation of water. Recently, it has been demonstrated in molecular beam experiments that the chromophores pyridine (Py) and pyrimidine (Pm) can catalytically photooxidize water molecules in hydrogen-bonded Py⋯$(H_2O)_n$ and Pm⋯$(H_2O)_n$ clusters via an excited-state proton-coupled electron transfer (PCET) reaction, resulting in the formation of PyH and PmH radicals, which were detected via their electronic spectra[34,35] (here and in the following the dots indicate a hydrogen bond). As radicals, PyH and PmH possess absorbing excited states in the visible range of the

[a] S. Pios, X. Huang, Prof. Dr. W. Domcke
Department of Chemistry
Technical University of Munich
85747 Garching (Germany)
E-mail: domcke@ch.tum.de

ChemPhotoChem

Articles
doi.org/10.1002/cptc.202000305

Chemistry
Europe
European Chemical
Societies Publishing

spectrum. It was shown computationally that these hypervalent radicals possess, in addition, low-lying dark excited states of $^2\pi\sigma^*$ character which are dissociative with respect to the NH bond distance.[35,36] These $^2\pi\sigma^*$ states can drive direct (non-statistical) photodetachment of the excess hydrogen atom from the PyH radical. This reaction could be experimentally detected in PyH···$(H_2O)_n$ clusters.[34] In sufficiently large clusters, metastable H_3O···$(H_2O)_n$ complexes are generated by the photodetachment reactions which are finite-size models of the hydrated electron in liquid water[19,20] as discussed above. The Py or Pm chromophores are regenerated by the photodetachment reaction and therefore are photocatalysts.

Py and Pm absorb in the far UV and therefore UV radiation is required for the generation of hydrated electrons from water with these photocatalysts. However, a larger N-heterocycle, heptazine (heptaazaphenalene or tri-*s*-triazine) absorbs strongly in the near UV and weakly even in the visible range of the spectrum.[37,38] Heptazine (Hz) is the monomer of the organic polymeric photocatalyst graphitic carbon nitride (g-C_3N_4) which is widely employed in current water splitting research.[39–42] It has been predicted by ab initio calculations that Hz photo-excited to the bright $^1\pi\pi^*$ state can abstract a hydrogen atom from water in Hz···$(H_2O)_n$ complexes via a PCET reaction, yielding heptazinyl (HzH) and OH radicals.[43] The formation of the latter was confirmed experimentally for a chemically stable derivative of Hz, trianisole-heptazine (TAHz), in aqueous solution[44] which indirectly confirms the formation of the TAHzH radical. The calculations predict that the low-lying bound $^2\pi\pi^*$ states of the HzH radical are predissociated by $^2\pi\sigma^*$ states which are repulsive with respect to the NH bond length, like in the PyH and PmH radicals.[43] In the present work, we explored with electronic-structure calculations the possibility of generation of hydrated hydronium radicals by the photodetachment of H-atoms from the HzH radical in water clusters. Scheme 1 illustrates the reaction cycle. Photo-induced H-atom abstraction from a hydrogen-bonded water molecule is the initial reaction (top). Photo-induced H-atom transfer from the HzH radical to a hydrogen-bonded water molecule generates the H_3O radical and regenerates the Hz molecule (bottom). Since the calculations with accurate wave-function-based ab initio methods are challenging due to the large size of the Hz chromophore, we restricted the calculations to the HzH···H_2O complex as the simplest system and to the HzH···$(H_2O)_4$ complex as a more realistic system. The transfer of the H-atom from HzH to $(H_2O)_4$ yields the H_3O···$(H_2O)_3$ complex, that is, the H_3O radical with a complete first solvation shell.

The excitation energy of the lowest bright $^1\pi\pi^*$ state of Hz and the excitation energies of the $^2\pi\pi^*$ states of HzH can systematically be lowered by substituents. For example, the excitation energy of the lowest bright state of TAHz is lower than the excitation energy of the lowest bright state of Hz by 0.8 eV.[45] The absorption spectra of Hz as well as of the HzH radical can be tuned into the visible by suitable substituents.[46] These considerations suggest that the formation of hydrated electrons from water with visible light may tentatively be possible.

Computational Methods

The ground-state equilibrium geometries of the HzH radical and the HzH···H_2O and HzH···$(H_2O)_4$ complexes were optimized with the unrestricted second-order Møller-Plesset (UMP2) method.[47] The UMP2 method is preferred here to the complete-active-space self-consistent-field (CASSCF) method[48] for geometry optimization, because dynamic electron correlation effects, which are relevant for the description of weak long-range interactions such as hydrogen bonds, are taken into account in the former. The higher accuracy of the UMP2 geometries was confirmed by selected geometry optimizations for HzH and HzH···H_2O with the CASPT2 method[49] (second-order perturbation theory with respect to the CASSCF reference). The electronic ground state wave function of the HzH radical is of A″ symmetry in the C_s symmetry group, since the unpaired electron occupies a π orbital. The equilibrium geometries of the HzH···H_2O and HzH···$(H_2O)_4$ complexes were optimized with C_s symmetry constraint. The H_2O molecule in the HzH···H_2O complex is constrained to lie perpendicular to the molecular plane of HzH and the H_2O molecules in the HzH···$(H_2O)_4$ complex are arranged symmetrically to the HzH molecular plane. The C_s symmetry constraint is essential for geometry optimizations in excited electronic states (see below), because the symmetry constraint prevents the collapse of the energy of the lowest A′ state to the energies of lower A″ states.
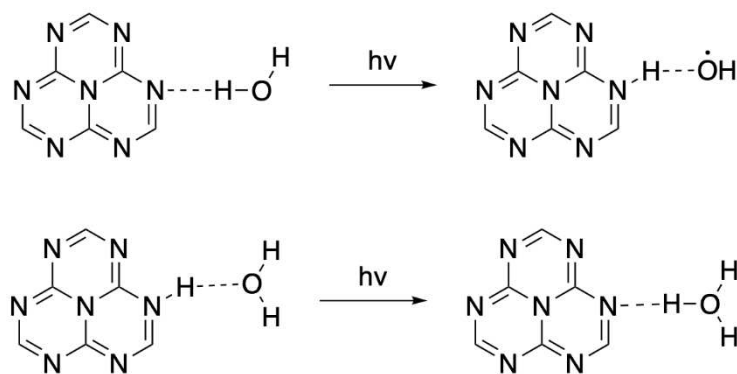
Scheme 1. Photocatalytic cycle of the generation of the H_3O radical from water in a two-photon reaction with the Hz chromophore. In the first photo-induced reaction (top), an H-atom is abstracted from a hydrogen-bonded water molecule by Hz. In the second photo-induced reaction (bottom), a H_3O radical is generated by H-atom transfer from the HzH radical to a hydrogen-bonded water molecule.

ChemPhotoChem

Articles
doi.org/10.1002/cptc.202000305

**Chemistry
Europe**

European Chemical
Societies Publishing

Vertical electronic excitation energies were calculated with the CASPT2 method. The active space for the CASSCF calculations for the HzH radical and its complexes with water consisted of seven active electrons distributed in nine orbitals, four π orbitals, four π^* orbitals and one σ^* orbital of HzH. In A″ symmetry, the CASSCF energy functional was averaged over the three lowest states of A″ symmetry. The energies of the lowest $^2\pi\pi^*$ states and $^2\pi\sigma^*$ states were found to be stable with respect to extensions of the active space. For the calculation of higher excited states of $^2\pi\pi^*$ character (D_4, D_5), the active space was extended by an additional π^* orbital and the D_1, D_2 states were not included in the state averaging. In the CASPT2 calculations, an imaginary denominator shift of 0.15 Hartree was chosen to mitigate intruder state problems.

For HzH and the HzH···H_2O complex, the augmented correlation-consistent polarized valence-split double-ζ basis set (aug-cc-pVDZ)[50] was employed. For geometry optimizations of the HzH···$(H_2O)_4$ complex, a partially augmented basis set was used. The non-augmented cc-pVDZ basis was employed on the HzH chromophore, while the aug-cc-pVDZ basis was chosen for the $(H_2O)_4$ cluster. The partial augmentation lowered the cost of the geometry optimizations considerably. The fully augmented basis was used for single-point energy calculations for the HzH···$(H_2O)_4$ complex. We tested the accuracy of the approximation of partial augmentation for selected optimized geometries. The differences of the geometries obtained with the partially augmented basis and the fully augmented basis were minimal.

The TURBOMOLE program package (V 6.3.1)[51] was employed for the UMP2 calculations, making use of the resolution-of-the-identity (RI) approximation. The OpenMolcas program package (V 18.09)[52] was used for the CASSCF and CASPT2 calculations.

The energy profiles for the photodissociation reaction of the HzH radical were computed along a rigid scan by stretching the NH bond length, keeping all other internal nuclear coordinates fixed at the UMP2-optimized ground-state equilibrium geometry. The photoinduced PCET reaction in the HzH···H_2O and HzH···$(H_2O)_4$ complexes was characterized by the calculation of minimum-energy paths as relaxed scans in the lowest $^2\pi\sigma^*$ excited state at the UMP2 level. For a fixed NH distance of HzH, the $^2\pi\sigma^*$ energy was optimized with respect to all other internal degrees of freedom of the complexes. In addition, the ground-state equilibrium geometries of the H-atom-transferred structures, Hz···H_3O and Hz···H_3O-$(H_2O)_3$, were fully optimized at the UMP2 level. Single-point energy calculations at the UMP2-optimized geometries were performed with the CASPT2 method. Such energies are referred to as UMP2//CASPT2 in what follows.

In addition, macroscopic solvent effects were taken into account using a polarizable continuum (PC) model described by Barone and Cossi and implemented in the OpenMolcas Package.[53,54] To simulate the macroscopic water environment, the dielectric constant was set to $\varepsilon = 78.39$. The continuum solvation shell was relaxed for the electronic ground state.

Finally, the dissociation energies of the Hz···H_3O and Hz···$H_3O(H_2O)_3$ complexes into Hz + H_3O and Hz + $H_3O(H_2O)_3$ were computed at the UMP2//CASPT2 level.

2. Results

2.1. The HzH Radical

The excited states of the HzH radical and the potential energy functions for the H-atom photodetachment reaction from HzH

were calculated by Ehrmaier et al.[43] with the UADC(2) method. Here, we briefly present results for the HzH photodissociation reaction obtained at the CASPT2 level as references for the H-atom transfer reactions in HzH-water complexes.

At the UMP2 level, the minimum energy configuration of the HzH radical exhibits a slight out-of-plane bending of the CH bond. The planar configuration (C_s symmetry) is a first-order saddle point. Since the stabilization of the ground-state energy by the slight out-of-plane bending of the NH group is minor, we choose the planar conformation as the reference geometry, because the excited-state calculations are greatly simplified by C_s symmetry. The NH bond length of planar HzH is 1.016 Å at the UMP2/aug-cc-pVDZ level. Since the singly occupied orbital (SOMO) is a π orbital of a″ symmetry, the electronic ground state of HzH is of A″ symmetry. The lowest unoccupied molecular orbital (LUMO) is a diffuse σ^* orbital of a′ symmetry and the $^2\pi\sigma^*$ excited state therefore is of A′ symmetry. The SOMO and the LUMO of HzH are displayed in Figures 1(b) and 1(a), respectively.

Whereas the highest occupied molecular orbital (HOMO) of Hz is localized on the peripheral N-atoms and the LUMO of Hz is located on the peripheral C-atoms and the central N-atom,[43] the SOMO of HzH is delocalized over both C-atoms and N-
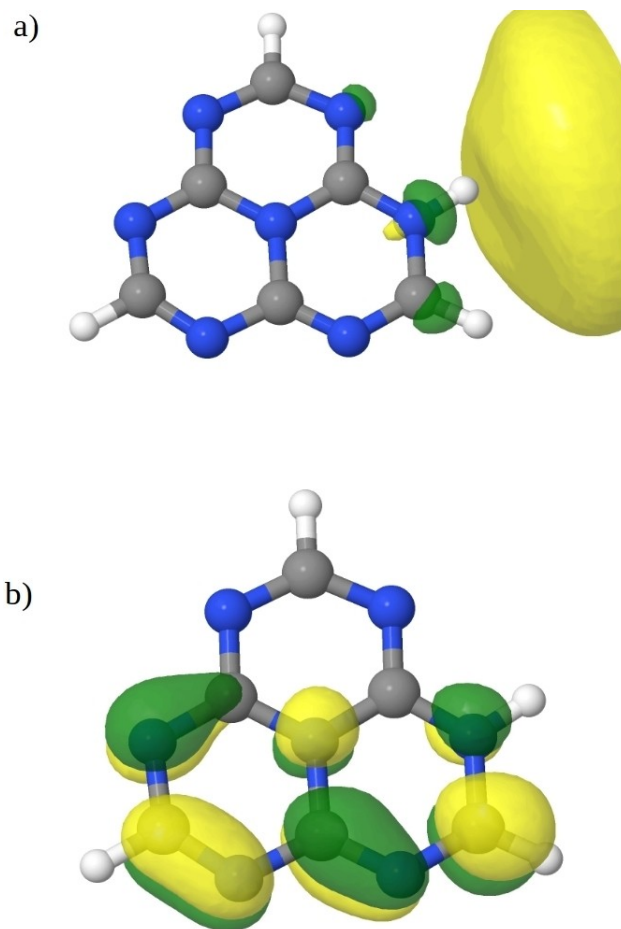
Figure 1. LUMO (a) and SOMO (b) of the HzH radical at its ground-state equilibrium structure.

ChemPhotoChem

Articles
doi.org/10.1002/cptc.202000305

**Chemistry
Europe**

European Chemical
Societies Publishing

atoms, see Figure 1(b). The structure of the LUMO is remarkable: the electronic density is to a large extent localized outside the molecular frame and the orbital is antibonding with respect to the NH bond (see Figure 1(a)). The SOMO-to-LUMO excitation is accompanied by a significant shift of the electronic charge from the aromatic ring beyond the H-atom of the NH group, which results in a significant dipole moment of the $\pi\sigma^*$ excited state (10.57 Debye). The vertical excitation energies of the lowest five excited states of HzH calculated with the CASPT2 method are listed in the left column of Table 1. The lowest two excited states (D_1, D_2), with excitation energies of 1.32 eV and 1.42 eV, are of $^2\pi\pi^*$ character, while the third excited state (D_3) is of $^2\pi\sigma^*$ character. The following two states (D_4, D_5) are again $^2\pi\pi^*$ states. The $^2\pi\pi^*$ states have non-vanishing, albeit small, oscillator strengths, while the $^2\pi\sigma^*$ state is dark due to the non-overlapping nature of SOMO and LUMO.

The potential-energy (PE) functions (calculated as rigid scans) for the H-atom abstraction reaction from HzH are shown in Figure 2. A relaxed scan yields essentially identical PE functions. While the PE functions of the $^2\pi\pi^*$ states D_1, D_2, D_4, D_5 are essentially parallel to the PE function of the electronic ground state, the PE function of the $^2\pi\sigma^*$ state is dissociative apart from a tiny barrier near $R_{NH} = 1.2$ Å. The $^2\pi\sigma^*$ energy intersects the energies of the D_1, D_2 excited states as well as the energy of the D_0 state. These curve crossings, which become conical intersections when out-of-plane vibrational modes are taken into account, provide a mechanism for predissociation of the $^2\pi\pi^*$ excited states as well as the electronic ground state of HzH.

The $^2\pi\sigma^*$ state of HzH dissociates homolytically into Hz and a neutral hydrogen atom, whereas the ground state and the $^2\pi\pi^*$ excited states dissociate heterolytically into ion pairs, the anion of Hz and a proton. The large dipole moment of the $^2\pi\sigma^*$ state at the ground-state equilibrium geometry decreases strongly with increasing R_{NH}, while the dipole moments of the ground state and the $^2\pi\pi^*$ excited states gradually increase with R_{NH}. This behaviour of the dipole moment functions is illustrated in Figure S1 of the supporting information.

The dissociation energy D_e of HzH is computed as 2.22 eV at the CASPT2 level, in good agreement with the estimate of 2.0 eV at the CCSD level.[43]
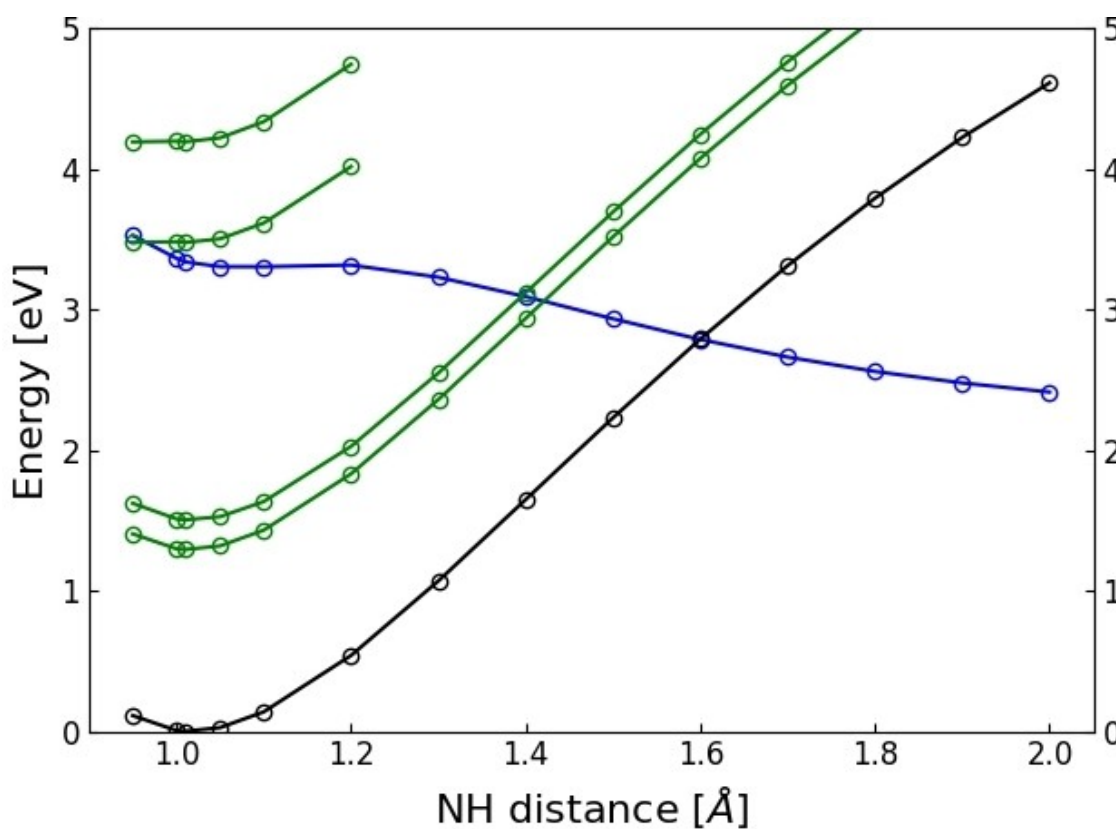
Table 1. Vertical excitation energies [eV], oscillator strengths f (in parentheses) and characters of the wave function (in brackets) of the five lowest excited states of the HzH, HzH···H_2O and HzH···$(H_2O)_4$ radicals at the CASPT2 level.

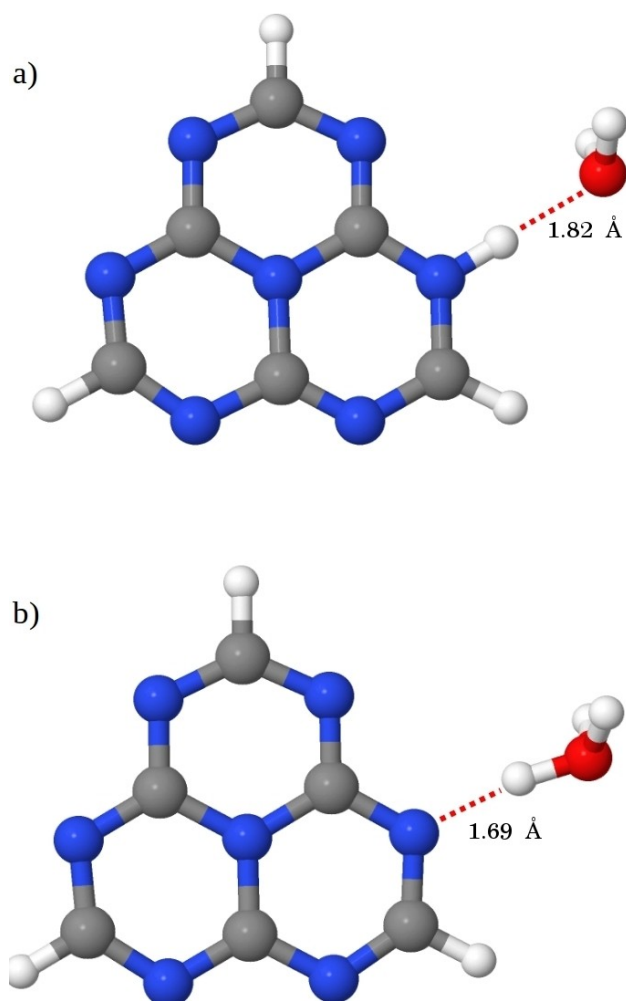| State	HzH	HzH–H_2O	HzH–$(H_2O)_4$
D_1	1.32 (0.025) [$\pi\pi^*$]	1.36 (0.053) [$\pi\pi^*$]	1.32 (0.052) [$\pi\pi^*$]
D_2	1.42 (0.013) [$\pi\pi^*$]	1.72 (0.018) [$\pi\pi^*$]	1.57 (0.018) [$\pi\pi^*$]
D_3	3.32 (0.000) [$\pi\sigma^*$]	3.36 (0.002) [$\pi\pi^*$]	3.39 (0.003) [$\pi\pi^*$]
D_4	3.48 (0.014) [$\pi\pi^*$]	3.50 (0.003) [$\pi\sigma^*$]	3.63 (0.001) [$\pi\sigma^*$]
D_5	4.13 (0.110) [$\pi\pi^*$]	4.07 (0.023) [$\pi\pi^*$]	3.93 (0.034) [$\pi\pi^*$]

Figure 2. Cut of the PE surfaces (rigid scan) of the HzH radical along the NH stretching coordinate at the CASPT2 level. Black: electronic ground state; green: $\pi\pi^*$ excited states; blue: $\pi\sigma^*$ excited state.

ChemPhotoChem

Articles
doi.org/10.1002/cptc.202000305

**Chemistry
Europe**
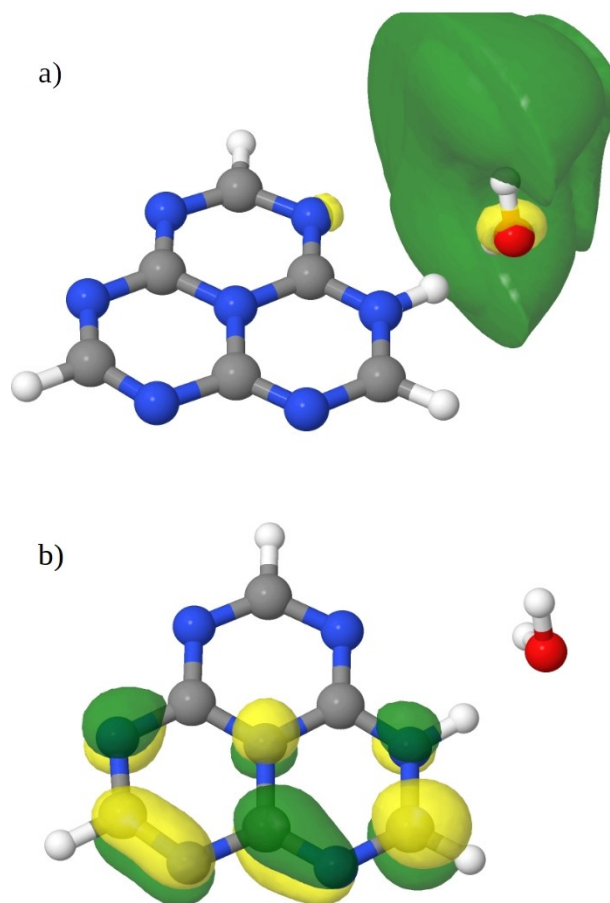European Chemical
Societies Publishing

2.2. The HzH···H₂O Complex

The ground-state equilibrium structure of the HzH···H₂O complex is shown in Figure 3(a). The NH bond length is 1.032 Å. The length of the NH···OH₂ hydrogen bond is 1.823 Å, which represents a rather strong hydrogen bond.

The frontier molecular orbitals (SOMO and LUMO) of the HzH···H₂O complex are displayed in Figure 4. Whereas the π-type SOMO is essentially unperturbed by the hydrogen bond with the H₂O molecule (Figure 4(b)), the σ*-type LUMO is strongly affected. It is pushed away from the aromatic frame and represents an external electron cloud which is solvated by the two OH bonds of the H₂O molecule (Figure 4(a)).

The vertical electronic excitation energies of the HzH···H₂O complex are listed in the middle column of Table 1. In HzH···H₂O, the $D_3(\pi\sigma^*)$ state is slightly destabilized, while the $D_4(\pi\pi^*)$ state is slightly stabilized with respect to the free HzH radical. As a result, the ordering of these closely spaced states is interchanged, see Table 1. The $D_2(\pi\pi^*)$ state exhibits the largest shift in energy ($+0.30$ eV) due to the hydrogen bonding of HzH with H₂O.
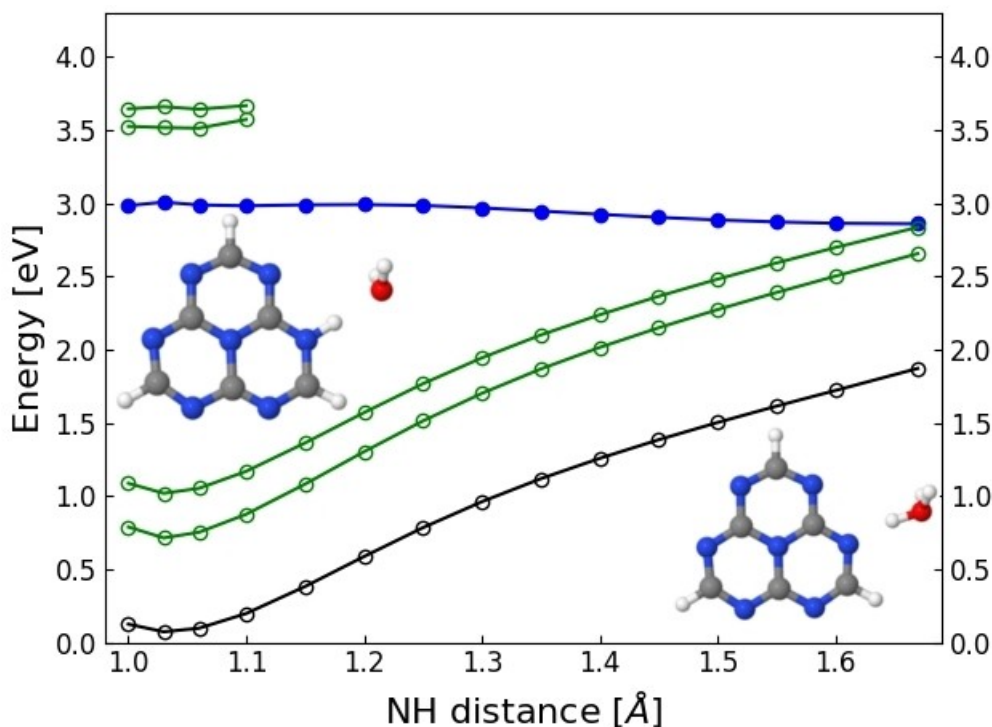
a)

b)

Figure 4. LUMO (a) and SOMO (b) of the HzH···H₂O complex at the ground-state equilibrium geometry.

a)

1.82 Å

b)

1.69 Å

Figure 3. (a) Ground-state equilibrium structure of the HzH···H₂O complex. (b) Ground-state equilibrium structure of the Hz···H₃O complex.

The CASPT2 PE profiles of the minimum-energy path (calculated as relaxed scan at the UMP2 level, see Section 2) for the excited-state PCET reaction from HzH to H₂O are shown in Figure 5. The energies of the D_0 state (black), the D_3 state of $^2\pi\sigma^*$ character (blue) and the D_1, D_2, D_4, D_5 states of $^1\pi\pi^*$ character (green) were computed with the CASPT2 method along the $^2\pi\sigma^*$-optimized reaction path. Compared with the PE functions of the H-atom detachment reaction in HzH (Figure 2), the $^2\pi\sigma^*$ PE function becomes somewhat less repulsive, while the PE profiles of the D_0 state and the $^2\pi\pi^*$ excited states become significantly less attractive. The stabilization of the energies of the D_0 state and the $^2\pi\pi^*$ states at large NH distances reflects the large energy gain by the formation of the H_3O^+ cation upon proton transfer from HzH to H₂O. While the D_0 energy of isolated HzH is about 3.5 eV at $R_{NH} = 1.7$ Å, the D_0 energy is lowered to 1.9 eV at $R_{NH} = 1.7$ Å in the HzH···H₂O complex. The PE profile of the $^2\pi\sigma^*$ state of HzH···H₂O, on the other hand, is lowered at short NH distances and raised at large NH distances and therefore flattened compared to the PE profile of HzH. This flattening in the HzH···H₂O complex is due to the decrease of the dipole moment of the $^2\pi\sigma^*$ state along the H-atom transfer reaction path, see Figure S1. While the $^2\pi\sigma^*$ state is highly polar at the ground-state equilibrium geometry of HzH···H₂O, it becomes nonpolar when Hz and the H₃O radical

ChemPhotoChem

Articles
doi.org/10.1002/cptc.202000305

Chemistry
Europe
European Chemical
Societies Publishing

Figure 5. Energy profiles of the relaxed scan of the HzH···H$_2$O complex along the NH-stretching coordinate. The minimum-energy path is optimized in the $\pi\sigma^*$ state at the UMP2 level. Energies are calculated with the CASPT2 method at the UMP2-optimized geometries. Black: electronic ground state; green: $\pi\pi^*$ states; blue: $\pi\sigma^*$ state. Full circles indicate that the reaction path geometry was optimized in this state; open circles indicate that the reaction path geometry was optimized in a different state.

are formed at large NH distances. The intersection of the $^2\pi\sigma^*$ energy function with the D$_0$ energy in free HzH disappears and the intersection of the $^2\pi\sigma^*$ energy with the D$_3(\pi\pi^*)$ energy is shifted outward to 1.7 Å, see Figure 5. As a result, there exists a barrierless reaction path for H-atom transfer in the $^2\pi\sigma^*$ state of the HzH···H$_2$O complex which leads to a conical intersection with the $^2\pi\pi^*$ state (D$_2$) at large NH distances (Figure 5).

The $^2\pi\sigma^*$ PE surface of the HzH···H$_2$O complex exhibits a very shallow minimum corresponding to a Hz···H$_3$O structure which is shown in Figure 3(b). The length of the N···HO hydrogen bond of this complex is 1.691 Å, shorter than the hydrogen bond in the HzH···H$_2$O complex (1.823 Å). The stabilization energy with respect to the vertical excitation energy of the $^2\pi\sigma^*$ state is 0.65 eV. The computed energy of dissociation of the Hz···H$_3$O complex into Hz and the H$_3$O radical is 0.30 eV. Vertical excitation of the $^2\pi\sigma^*$ state in HzH···H$_2$O complexes will therefore likely lead to H-atom transfer.
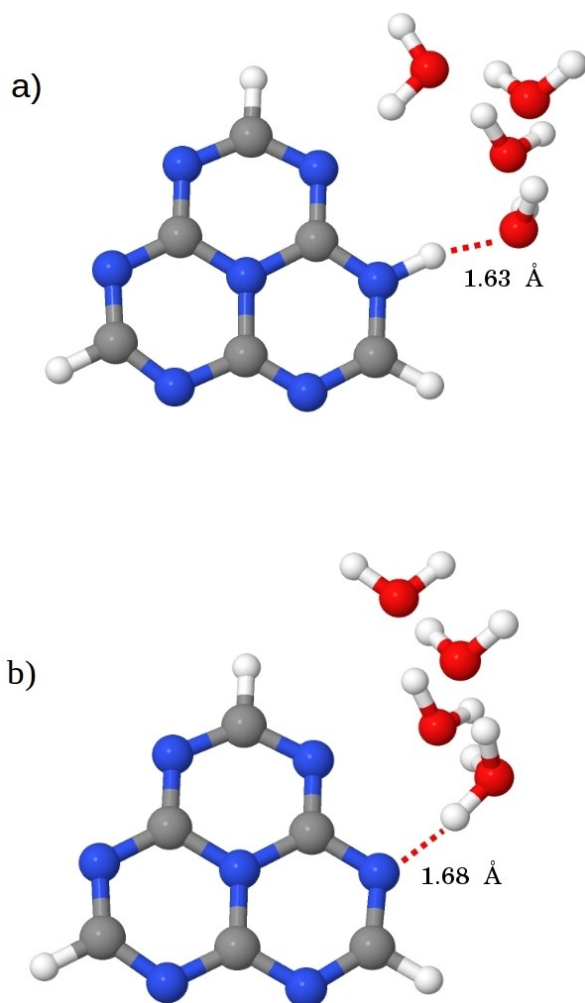
2.3. The HzH···(H$_2$O)$_4$ Complex

The ground-state geometry of the HzH···(H$_2$O)$_4$ complex was optimized at the UMP2 level with C$_s$ symmetry constraint. While there exist a large number of possible equilibrium structures of this complex, the structure of the water cluster has been chosen such that the H$_2$O molecule in the first solvation shell is bonded as H-atom acceptor to the NH group of HzH. The two

OH bonds of this H$_2$O molecule form hydrogen bonds to two H$_2$O molecules in the second solvation shell. The fourth H$_2$O molecule forms a weak hydrogen bond with the N-atom adjacent to the NH group of HzH, see Figure 6(a). The length of the hydrogen bond between the NH group of HzH and the closest water molecule is 1.632 Å. The significant shortening of this hydrogen bond compared to the Hz···H$_2$O complex (1.823 Å) indicates a significant strengthening of the HzH···H$_2$O hydrogen bond in the larger complex.

The π-type SOMO of the HzH···(H$_2$O)$_4$ complex at the ground-state equilibrium geometry is essentially the same as that of the free HzH radical. The LUMO of σ^* character of the HzH···(H$_2$O)$_4$ complex is depicted in Figure 7. It is localized outside the water cluster and solvated by free OH bonds of water molecules in the second and third solvation shell. The $^2\pi\sigma^*$ state of HzH···(H$_2$O)$_4$ is thus a spontaneously charge-separated state, consisting of a protonated Hz molecule and a finite-size solvated electron.

The vertical excitation energies of the HzH···(H$_2$O)$_4$ complex are listed in the third column of Table 1. The $^2\pi\pi^*$ vertical excitation energies of the HzH chromophore are only weakly affected by the aqueous microenvironment. The $^2\pi\sigma^*$ excited state is blue shifted by about 0.30 eV in HzH···(H$_2$O)$_4$ relative to HzH.
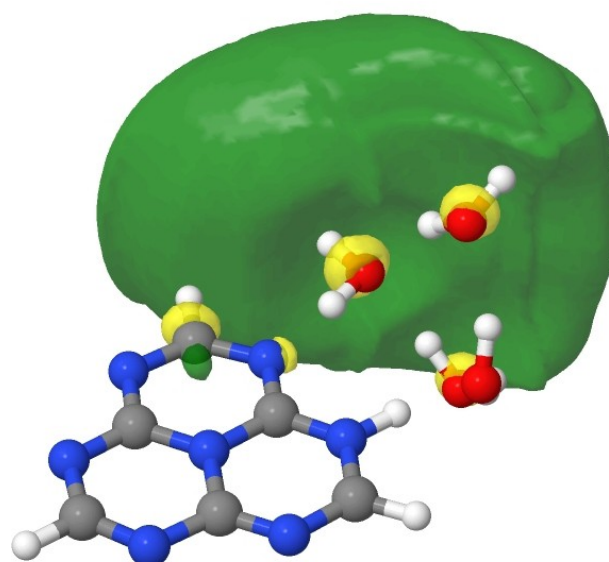
The energy profiles of the relaxed scan for H-atom transfer from HzH to the (H$_2$O)$_4$ cluster are displayed in Figure 8. The rearrangement of the nuclear geometry by minimization of the $^2\pi\sigma^*$ energy raises the energies of the D$_0$ state and the $^2\pi\pi^*$

ChemPhotoChem

Articles
doi.org/10.1002/cptc.202000305

Chemistry
Europe
European Chemical
Societies Publishing

Figure 6. (a) Ground-state equilibrium structure of the HzH···(H$_2$O)$_4$ complex. (b) Ground-state equilibrium structure of the Hz···H$_3$O(H$_2$O)$_3$ complex. Both structures were optimized at the UMP2 level.

Figure 7. LUMO of the HzH···(H$_2$O)$_4$ radical at its ground-state equilibrium structure.

states at short NH distances ($R_{NH} \approx 1.0$ Å). At large NH distances ($R_{NH} \approx 1.7$ Å), the energies of these states are stabilized with respect to the HzH···H$_2$O complex by more than 0.5 eV. As a result, the PE profiles of the D$_0$ state and the $^2\pi\pi^*$ states of HzH···(H$_2$O)$_4$ (Figure 8) are considerably flattened in comparison with HzH···H$_2$O (Figure 5) which reflects the stabilization of the ionic D$_0$ and $^2\pi\pi^*$ states by the water cluster. The energy profile of the $^2\pi\sigma^*$ state is more repulsive in the HzH···(H$_2$O)$_4$ complex than in the HzH···H$_2$O complex due to a slight destabilization of the $^2\pi\sigma^*$ energy at short NH distances and a slight stabilization at large NH distances (see Figure 8). Remarkably, all crossings of the $^2\pi\sigma^*$ energy with the energies of the lower-lying states (D$_0$, D$_1$, D$_2$) have been eliminated by the larger water environment. The formation of the Hz···H$_3$O(H$_2$O)$_3$ complex from the $^2\pi\sigma^*$ excited state of the HzH···(H$_2$O)$_4$ complex is found to be a barrierless adiabatic PCET reaction without perturbation by energy crossings, in remarkable contrast to the H-atom photodetachment reaction from HzH (Figure 2).

Figure 9 shows the same energy profiles as in Figure 8, but with inclusion of macroscopic electronic solvation effects with

the polarized continuum model. The PE functions become even flatter than in the isolated HzH···(H$_2$O)$_4$ complex. The stabilization energy of the $^2\pi\sigma^*$ state due to H-atom transfer is reduced to 0.16 eV. The energy-gap between the $^2\pi\sigma^*$ state and the D$_2$ state increases to 1.95 eV at large NH distances.

The energy of dissociation of the Hz···H$_3$O(H$_2$O)$_3$ complex into Hz and H$_3$O···(H$_2$O)$_3$ is computed as 0.67 eV with C$_s$ symmetry constraint. When the symmetry constraint is relaxed for the free H$_3$O(H$_2$O)$_3$ radical, the dissociation energy increases to 0.79 eV. The binding energy of the Hz···H$_3$O(H$_2$O)$_3$ product is thus larger than the excess energy of the PCET reaction in the $^2\pi\sigma^*$ state. When the HzH···(H$_2$O)$_4$ complex is excited to the D$_4$ or D$_5$ states, followed by radiationless relaxation to the D$_3(\pi\sigma^*)$ state, the excess energies of the radiationless decay and the PCET reaction in the $^2\pi\sigma^*$ state together are sufficient to allow the dissociation of the complex into Hz and H$_3$O(H$_2$O)$_3$, that is, the formation of a free hydrated electron.

3. Discussion

It is interesting to compare the H-atom photodetachment reaction in HzH and the excited-state H-atom transfer reaction in HzH···(H$_2$O)$_n$ complexes with the corresponding reactions in typical closed-shell photoacids and their hydrogen-bonded complexes with water molecules, because a large amount of experimental and computational data is available for closed-shell photoacids, whereas experimental data for open-shell photoacids like PyH, PmH or HzH are extremely scarce. The kinetic energy distributions of H-atoms photodetached from pyrrole, phenol, indole, thiophenol, etc., were extensively investigated with velocity map imaging, multimass ion imaging, Rydberg tagging and femtosecond spectroscopy experiments, see[55–60] for representative examples. These experimen-
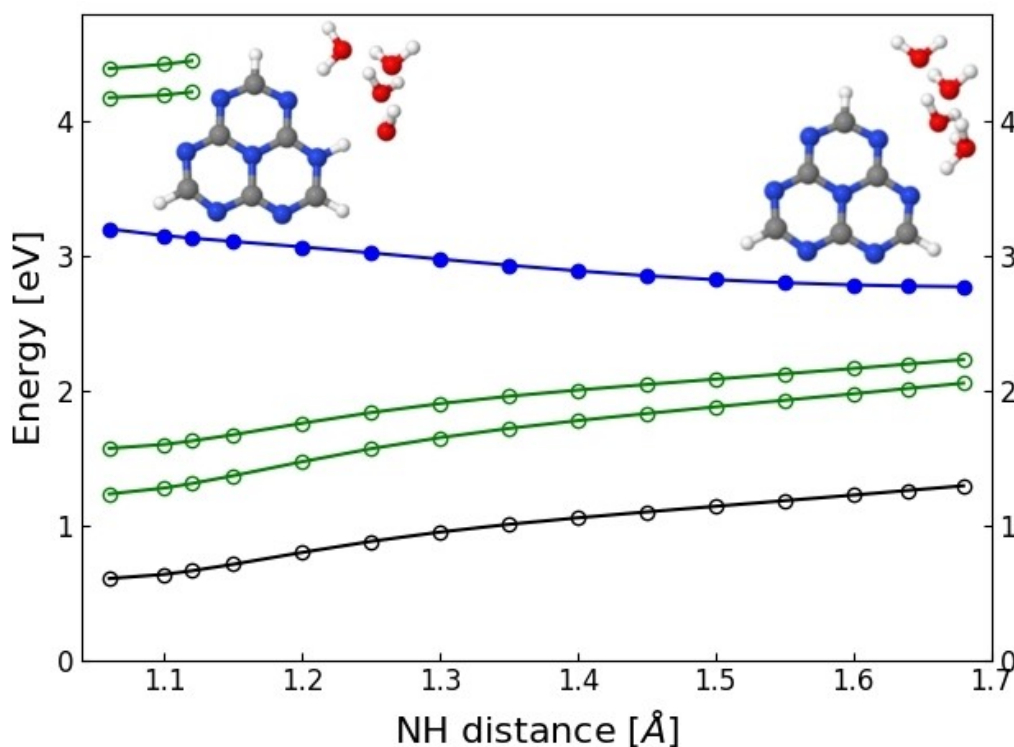
Figure 8. Energy profiles of the relaxed scan of the HzH···(H₂O)₄ complex along the NH-stretching coordinate. The minimum-energy path is optimized in the πσ* state at the UMP2 level. Energies are calculated with the CASPT2 method at the UMP2-optimized geometries. Black: electronic ground state; green: ππ* states; blue: πσ* state. Full circles indicate that the reaction path geometry was optimized in this state; open circles indicate that the reaction path geometry was optimized in a different state.

tal studies were supported by ab initio calculations of the relevant PE surfaces and by calculations of the nonadiabatic time-dependent quantum wave-packet dynamics, e.g.[61–67] or quasi-classical trajectory surface-hopping simulations, e.g..[68–73] For phenol···(NH₃)ₙ, phenol···(H₂O)ₙ and pyrrole···(NH₃)ₙ complexes, it was experimentally established that PCET from photoexcited pyrrole or phenol to the solvent molecules is the dominant process,[74–77] rather than proton transfer, as previously thought.[78,79]

The shape of the diffuse σ* orbital located on the NH group of HzH is similar to the shape of the σ* orbitals of pyrrole, phenol and indole.[19] Upon extension of the NH or OH bond of these photoacids, the σ* orbital collapses to the compact 1 s orbital of the free H-atom, which is the reason for the pronounced stabilization of the πσ* energy by NH or OH bond stretching.[19] The vertical electronic excitation spectrum of HzH exhibits similarities with the excitation spectrum of indole (two absorbing ππ* states, followed by a dark πσ* state),[80] but the excitation energies of HzH are much lower, as expected for a radical. The PE crossings along the NH stretching coordinate in HzH also are qualitatively similar to indole, but are located at much lower electronic excitation energies. While the vertical excitation energies of the L_a, L_b states of indole are ≈ 4.5 eV, the excitation energies of the D_1, D_2 states of HzH are 1.3 −1.4 eV. The vertical excitation energy of the πσ* state of indole is about 5.0 eV, while it is about 3.3 eV in HzH. The energy of the ¹πσ*-S_0 energy crossing is at ≈ 4.6 eV in indole,

while the energy of the ²πσ*-D_0 crossing is at ≈ 2.7 eV in HzH. The photodissociation of HzH can thus be driven by near-UV photons (≈ 3.5 eV, the vertical excitation energy of the D_4 state), whereas the excitation threshold for photodissociation of indole is 1.5 eV higher (≈ 5.0 eV).

The electronic structure of the ²πσ* state of the HzH···(H₂O)₄ complex is analogous to that found for the indole···(H₂O)ₙ or phenol···(H₂O)ₙ complexes.[81,82] In particular, the expulsion of the σ* orbital in the HzH···H₂O complex (Figure 4(a)) is similar to that found in the indole···H₂O and phenol···H₂O complexes. The σ* orbital of the πσ* excited state of HzH is squeezed out of the chromophore-water complex due to the strong and short hydrogen bonds between HzH and the water molecules and the electrophobic character of the H₂O molecule.[19]

Compared to the S_1(ππ*) state in the phenol···H₂O complex, the D_1(ππ*) and D_2(ππ*) states in the HzH···H₂O complex are much lower in energy and the ²πσ*-²ππ* energy crossing occurs at much larger bond distances. Like in phenol···(H₂O)ₙ complexes,[80,82] the conical intersection of the energy of the πσ* state with the energy of the electronic ground state along the H-atom detachment coordinate, which exists in free phenol and free HzH, is eliminated in the HzH···H₂O and HzH···(H₂O)₄ complexes. Phenol and indole are known as photoacids with a comparatively high yield of hydrated electrons when excited to their S_1 or S_2 states.[25,26] It can be expected that the absence of crossings of the ²πσ* energy with the energies of lower-lying electronic states in the HzH···(H₂O)₄ complex likewise may result
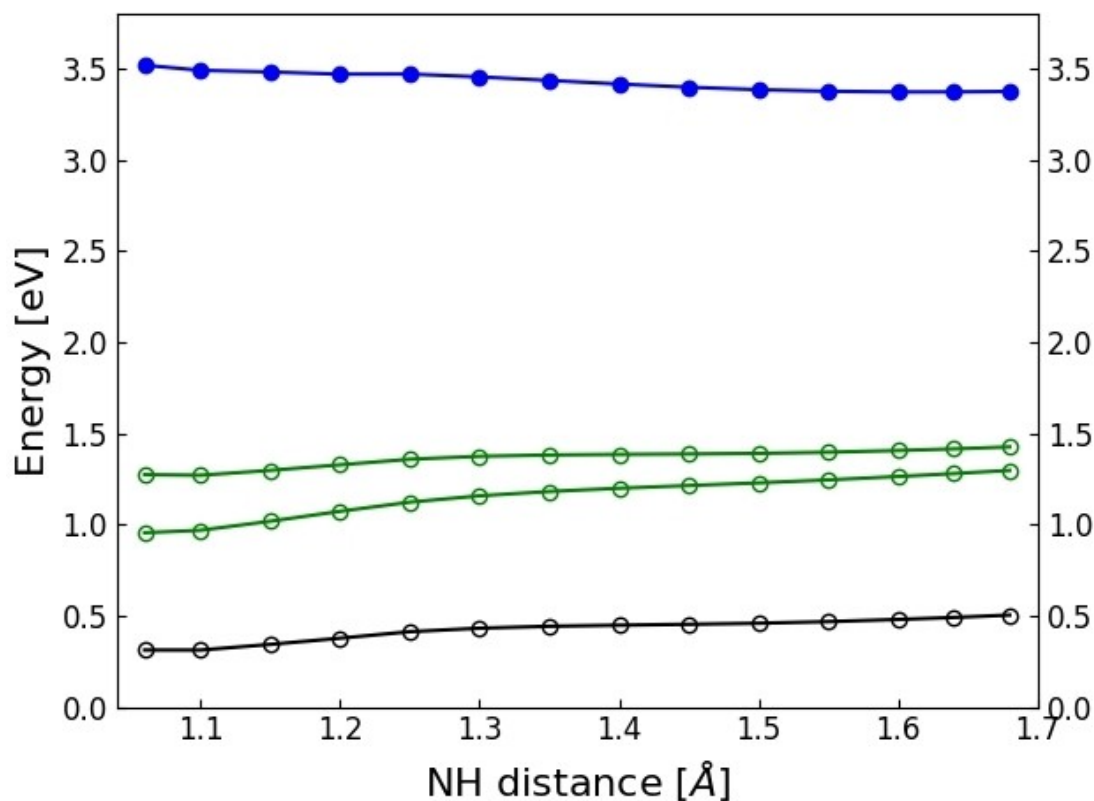
Figure 9. Energy profiles of the relaxed scan of the HzH⋯(H$_2$O)$_4$ complex along the NH-stretching coordinate. The minimum-energy path is optimized in the $\pi\sigma^*$-state at the UMP2 level. Energies are calculated at the UMP2-optimized geometries with the CASPT2 method including a polarizable continuum. Black: electronic ground state; green: $\pi\pi^*$ states; blue: $\pi\sigma^*$ state.

in a relatively high branching ratio for the formation of the of H$_3$O(H$_2$O)$_3$ radical.

The $^2\pi\sigma^*$ state of HzH can be populated by near-UV light either directly (due to vibronic intensity borrowing from allowed $^2\pi\pi^*$ states) or indirectly (by radiationless decay from the dense manifold of higher $^2\pi\pi^*$ states). The photodissociation of isolated HzH involves conical intersections of the $^2\pi\sigma^*$ state with two closely spaced low-lying $^2\pi\pi^*$ states and with the D$_0$ state, see Figure 2. At these conical intersections, a bifurcation of the nuclear dynamics will occur. Diabatic passage through the intersections leads to the detachment of free H-atoms, while adiabatic passage transfers the $^2\pi\sigma^*$ population to the bound $^2\pi\pi^*$ states and the D$_0$ state, which ultimately leads to relaxation to the energy minimum of the D$_0$ state, that is, aborted photodissociation. This kind of nonadiabatic photodissociation dynamics was investigated in a reduced-dimensional ab initio wave-packet dynamics study for the PyH radical, in which the PE function for NH dissociation in the $^2\pi\sigma^*$ state crosses the energy of a bound low-lying $^2\pi\pi^*$ state as well as the energy of the D$_0$ state. Dissociation yields of 33–90% were predicted for this system, depending on the initial preparation of the wave packet in the $^2\pi\sigma^*$ state.[83] The conical intersections thus act as quenchers of the photodissociation yield of the PyH radical.

As discussed above, the PE functions for H-atom transfer in the HzH⋯H$_2$O complex differ substantially from those for the photodetachment reaction in isolated HzH. Comparing Figure 2

and Figure 5, it is seen that the PE function of the $^2\pi\sigma^*$ state is less repulsive in the HzH⋯H$_2$O complex and the energies of the $^2\pi\pi^*$ states and the D$_0$ state are substantially lowered at large NH distances due to the formation of the strongly bound H$_3$O$^+$ cation. The conical intersection of the $^2\pi\sigma^*$ state with the D$_2(\pi\pi^*)$ state is shifted from ≈ 1.4 Å to ≈ 1.7 Å and the conical intersection with the D$_0$ state is eliminated altogether. When three more water molecules are added, the driving force for dissociation in the $^2\pi\sigma^*$ state slightly increases and the energies of the $^2\pi\pi^*$ states and the D$_0$ state are additionally lowered by about 0.6 eV at large NH distances (see Figure 8). The approximate inclusion of the effect of a macroscopic aqueous environment results in a further significant increase of the energy-gap between the $^2\pi\sigma^*$ state and the lower-lying $^2\pi\pi^*$ and D$_0$ states at large NH distances (Figure 9). As a result, all conical intersections which are involved in the photodissociation of the free HzH radical along the NH dissociation coordinate are eliminated in the HzH⋯(H$_2$O)$_4$ complex.

Although the energy of the ionic Hz$^-$⋯H$_3$O$^+$(H$_2$O)$_n$ ground state is lower than the energy of the neutral Hz⋯H$_3$O(H$_2$O)$_n$ radical, the relatively large energy gap between these ⋯states suppresses the nonadiabatic back-transfer of the electron to an extent that the separation of the H$_3$O(H$_2$O)$_n$ cluster from the Hz molecule can efficiently compete with the quenching of the excited state by electron back-transfer, which may result in a reasonably high quantum yield of formation of the hydrated electron. This conjecture should be confirmed by ab initio

ChemPhotoChem

Articles
doi.org/10.1002/cptc.202000305

Chemistry Europe
European Chemical
Societies Publishing

nonadiabatic dynamics simulations which, however, are challenging because of the electronic open-shell character of the $HzH\cdots(H_2O)_n$ system.

4. Conclusions

We explored the possibility of generating H_3O and OH radicals from water via photocatalytic reactions driven by the absorption of two near-UV/visible photons by the Hz chromophore. In the initial photoreaction, a Hz molecule is photoexcited and abstracts a hydrogen atom from a hydrogen-bonded water molecule in an excited-state PCET reaction. The feasibility of this reaction depends primarily on the barrier of the H-atom transfer reaction in the long-lived $S_1(\pi\pi^*)$ state of Hz, as discussed in detail in recent publications.[43,45,46] In the second photoreaction, the excess hydrogen atom of the HzH radical is transferred to the water environment as discussed in the present work. In this reaction, the electron in the π-type SOMO of the HzH radical is photoexcited to a σ^*-type orbital which drives a barrierless transfer of the excess hydrogen atom of HzH to a hydrogen-bonded water molecule, generating a hydrated H_3O radical. By this sequence of two PCET reactions, a water molecule is decomposed into a pair of (solvated) OH and H_3O radicals and the Hz chromophore is regenerated. The OH radicals have to be scavenged and recombined to H_2O_2 or $H_2O + O_2$ by a suitable co-catalyst. The hydrated H_3O radical is the energy-rich agent which is able to reduce ubiquitous feedstock molecules (like CO_2 or N_2) to clean fuels.[28–33] The realization of this scenario could potentially lead to an ultimately "green" pathway to renewable fuels, in which neither high temperatures nor high pressures are required.

A decisive advantage of organic photocatalysts compared with inorganic semiconductors is the ease of tuning of the absorption spectrum. There are various possibilities of shifting the absorption maximum of the lowest bright $^1\pi\pi^*$ state of Hz-based chromophores towards the visible spectrum as well as of increasing the oscillator strength of this state.[45,46] The reduced Hz chromophore (HzH) inherently absorbs in the visible. Exploratory computational screening studies are underway in our laboratory to identify Hz-based chromophores with optimal properties for driving PCET reactions in pure water with visible light.

Acknowledgements

Conflict of Interest

The authors declare no conflict of interest.

[1] E. J. Hart, J. W. Boag, *J. Am. Chem. Soc.* **1962**, *84*, 4090–4095.
[2] E. J. Hart, M. Anbar, *The Hydrated Electron*, Wiley, New York, **1970**.
[3] G. V. Buxton, C. L. Greenstock, W. P. Helman, A. B. Ross, *J. Phys. Chem. Ref. Data* **1988**, *17*, 513–531.
[4] B. Abel, U. Buck, A. L. Sobolewski, W. Domcke, *Phys. Chem. Chem. Phys.* **2012**, *14*, 22–34.
[5] J. M. Herbert, M. P. Coons, *Annu. Rev. Phys. Chem.* **2017**, *68*, 447–472.
[6] J. M. Herbert, *Phys. Chem. Chem. Phys.* **2019**, *21*, 20538–20565.
[7] D.-F. Feng, L. Kevan, *Chem. Rev.* **1980**, *80*, 1–20.
[8] P. J. Rossky, J. Schnitker, *J. Phys. Chem.* **1988**, *92*, 4277–4285.
[9] R. E. Larsen, W. J. Glover, B. J. Schwartz, *Science* **2010**, *329*, 65–69.
[10] J. M. Herbert, L. D. Jacobson, *J. Phys. Chem. A* **2011**, *115*, 14470–14483.
[11] R. Ludwig, D. Paschek, *ChemPhysChem* **2011**, *12*, 75–77.
[12] L. Turi, P. J. Rossky, *Chem. Rev.* **2012**, *112*, 5614–5674.
[13] F. Uhlig, O. Marsalek, P. Jungwirth, *J. Phys. Chem. Lett.* **2012**, *3*, 3071–3075.
[14] J. R. Casey, A. Kahros, B. J. Schwartz, *J. Phys. Chem. B* **2013**, *117*, 14173–14182.
[15] J. Wilhelm, J. VandeVondele, V. V. Rybkin, *Angew. Chem. Int. Ed.* **2019**, *58*, 3890–3893; *Angew. Chem.* **2019**, *131*, 3930–3933.
[16] S. Dasgupta, B. Rana, J. M. Herbert, *J. Phys. Chem. B* **2019**, *123*, 8074–8085.
[17] H. F. Hameka, G. W. Robinson, C. J. Marsden, *J. Phys. Chem.* **1987**, *91*, 3150–3157.
[18] J. T. R. Tuttle, S. Golden, *J. Phys. Chem.* **1991**, *95*, 5725–5736.
[19] A. L. Sobolewski, W. Domcke, C. Dedonder-Lardeux, C. Jouvet, *Phys. Chem. Chem. Phys.* **2002**, *4*, 1093–1100.
[20] F. Uhlig, O. Marsalek, P. Jungwirth, *Phys. Chem. Chem. Phys.* **2011**, *13*, 14003–14009.
[21] V. Svoboda, R. Michiels, A. C. LaForge, J. Med, F. Stienkemeier, P. Slavíček, H. J. Wörner, *Sci. Adv.* **2020**, *6*, eaaz0385.
[22] X. Chen, S. E. Bradforth, *Annu. Rev. Phys. Chem.* **2008**, *59*, 203–231.
[23] L. I. Grossweiner, G. Swenson, E. F. Zwicker, *Science* **1963**, *141*, 805–806.
[24] H.-I. Joschek, L. I. Grossweiner, *J. Am. Chem. Soc.* **1966**, *88*, 3261–3268.
[25] D. V. Bent, E. Hayon, *J. Am. Chem. Soc.* **1975**, *97*, 2606–2612.
[26] D. V. Bent, E. Hayon, *J. Am. Chem. Soc.* **1975**, *97*, 2599–2606.
[27] G. M. Roberts, H. J. B. Marroux, M. P. Grubb, M. N. R. Ashfold, A. J. Orr-Ewing, *J. Phys. Chem. A* **2014**, *118*, 11211–11225.
[28] R. J. Hamers, J. A. Bandy, D. Zhu, L. Zhang, *Faraday Discuss.* **2014**, *172*, 397–411.
[29] L. Zhang, D. Zhu, G. M. Nathanson, R. J. Hamers, *Angew. Chem. Int. Ed.* **2014**, *53*, 9746–9750; *Angew. Chem.* **2014**, *126*, 9904–9908.
[30] L. Zhang, R. J. Hamers, *Diamond Relat. Mater.* **2017**, *78*, 24–30.
[31] D. Zhu, L. Zhang, R. E. Ruther, R. J. Hamers, *Nat. Mater.* **2013**, *12*, 836–841.
[32] J. R. Christianson, D. Zhu, R. J. Hamers, J. R. Schmidt, *J. Phys. Chem. B* **2014**, *118*, 195–203.
[33] J. A. Bandy, D. Zhu, R. J. Hamers, *Diamond Relat. Mater.* **2016**, *64*, 34–41.
[34] N. Esteves-Lopez, S. Coussan, C. Dedonder-Lardeux, C. Jouvet, *Phys. Chem. Chem. Phys.* **2016**, *18*, 25637–25644.
[35] X. Huang, J.-P. Aranguren, J. Ehrmaier, J. A. Noble, W. Xie, A. L. Sobolewski, C. Dedonder-Lardeux, C. Jouvet, W. Domcke, *Phys. Chem. Chem. Phys.* **2020**, *22*, 12502–12514.
[36] X. Liu, A. L. Sobolewski, R. Borrelli, W. Domcke, *Phys. Chem. Chem. Phys.* **2013**, *15*, 5957–5966.
[37] R. S. Hosmane, M. A. Rossmann, N. J. Leonard, *J. Am. Chem. Soc.* **1982**, *104*, 5497–5499.
[38] W. Leupin, J. Wirz, *J. Am. Chem. Soc.* **1980**, *102*, 6068–6075.
[39] X. Wang, K. Maeda, A. Thomas, K. Takanabe, G. Xin, J. M. Carlsson, K. Domen, M. Antonietti, *Nat. Mater.* **2009**, *8*, 76–80.
[40] Y. Wang, X. Wang, M. Antonietti, *Angew. Chem. Int. Ed.* **2012**, *51*, 68–89; *Angew. Chem.* **2012**, *124*, 70–92.
[41] W.-J. Ong, L.-L. Tan, Y. H. Ng, S.-T. Yong, S.-P. Chai, *Chem. Rev.* **2016**, *116*, 7159–7329.
[42] X. Wen, J. Xie, X. Chen, X. Li, *Appl. Surf. Sci.* **2017**, *391*, 72–123.
[43] J. Ehrmaier, T. N. Karsili, A. L. Sobolewski, W. Domcke, *J. Phys. Chem. A* **2017**, *121*, 4754–4764.
[44] E. J. Rabe, K. L. Corp, A. L. Sobolewski, W. Domcke, C. W. Schlenker, *J. Phys. Chem. Lett.* **2018**, *9*, 6257–6261.

ChemPhotoChem

Articles
doi.org/10.1002/cptc.202000305

Chemistry Europe
European Chemical
Societies Publishing

[45] W. Domcke, A. L. Sobolewski, C. W. Schlenker, *J. Chem. Phys.* **2020**, *153*, 100902.

[46] J. Ehrmaier, X. Huang, E. J. Rabe, K. L. Corp, C. W. Schlenker, A. L. Sobolewski, W. Domcke, *J. Phys. Chem. A* **2020**, *124*, 3698–3710.

[47] C. Møller, M. S. Plesset, *Phys. Rev.* **1934**, *46*, 618–622.

[48] R. Shepard, *Adv. Chem. Phys.* **1987**, *69*, 399–445.

[49] B. O. Roos, *Acc. Chem. Res.* **1999**, *32*, 137–144.

[50] T. H. Dunning Jr, *J. Chem. Phys.* **1989**, *90*, 1007–1023.

[51] TURBOMOLE V. 6.3.1; a development of University of Karlsruhe and Forschungszentrum Karlsruhe GmbH, 1989–2011; TURBOMOLE GmbH since 2007; available from http://www.turbomole.com **2007**.

[52] I. Fdez. Galván, M. Vacher, A. Alavi, C. Angeli, F. Aquilante, J. Autschbach, J. J. Bao, S. I. Bokarev, N. A. Bogdanov, R. K. Carlson, L. F. Chibotaru, J. Creutzberg, N. Dattani, M. G. Delcey, S. S. Dong, A. Dreuw, L. Freitag, L. M. Frutos, L. Gagliardi, F. Gendron, A. Giussani, L. González, G. Grell, M. Guo, C. E. Hoyer, M. Johansson, S. Keller, S. Knecht, G. Kovačević, E. Källman, G. Li Manni, M. Lundberg, Y. Ma, S. Mai, J. P. Malhado, P. Å. Malmqvist, P. Marquetand, S. A. Mewes, J. Norell, M. Olivucci, M. Oppel, Q. M. Phung, K. Pierloot, F. Plasser, M. Reiher, A. M. Sand, I. Schapiro, P. Sharma, C. J. Stein, L. K. Sørensen, D. G. Truhlar, M. Ugandi, L. Ungur, A. Valentini, S. Vancoillie, V. Veryazov, O. Weser, T. A. Wesołowski, P.-O. Widmark, S. Wouters, A. Zech, J. P. Zobel, R. Lindh, *J. Chem. Theory Comput.* **2019**, *15*, 5925–5964.

[53] V. Barone, M. Cossi, *J. Phys. Chem. A* **1998**, *102*, 1995–2001.

[54] M. Cossi, N. Rega, G. Scalmani, V. Barone, *J. Chem. Phys.* **2001**, *114*, 5691–5701.

[55] J. Wei, A. Kuczmann, F. Renth, F. Temps, *Phys. Chem. Chem. Phys.* **2003**, *5*, 315–320.

[56] C.-M. Tseng, Y. T. Lee, C.-K. Ni, *J. Chem. Phys.* **2004**, *121*, 2459–2461.

[57] B. Cronin, M. G. D. Nix, R. H. Qadiri, M. N. R. Ashfold, *Phys. Chem. Chem. Phys.* **2004**, *6*, 5031–5041.

[58] M. G. D. Nix, A. L. Devine, B. Cronin, M. N. R. Ashfold, *Phys. Chem. Chem. Phys.* **2006**, *8*, 2610–2618.

[59] M. G. D. Nix, A. L. Devine, B. Cronin, R. N. Dixon, M. N. R. Ashfold, *J. Chem. Phys.* **2006**, *125*, 133318.

[60] G. M. Roberts, V. G. Stavros, *Chem. Sci.* **2014**, *5*, 1698–1722.

[61] Z. Lan, W. Domcke, V. Vallet, A. L. Sobolewski, S. Mahapatra, *J. Chem. Phys.* **2005**, *122*, 224315.

[62] V. Vallet, Z. Lan, S. Mahapatra, A. L. Sobolewski, W. Domcke, *J. Chem. Phys.* **2005**, *123*, 144307.

[63] H. An, K. K. Baeck, *J. Phys. Chem. A* **2011**, *115*, 13309–13315.

[64] S. Faraji, M. Vazdar, V. S. Reddy, M. Eckert-Maksic, H. Lischka, *J. Chem. Phys.* **2011**, *135*, 154310.

[65] C. Xie, J. Ma, X. Zhu, D. R. Yarkony, D. Xie, H. Guo, *J. Am. Chem. Soc.* **2016**, *138*, 7828–7831.

[66] D. Picconi, S. Y. Grebenshchikov, *J. Chem. Phys.* **2018**, *148*, 104104.

[67] C. Xie, B. Zhao, C. L. Malbon, D. R. Yarkony, D. Xie, H. Guo, *J. Phys. Chem. Lett.* **2020**, *11*, 191–198.

[68] M. Barbatti, M. Vazdar, A. J. A. Aquino, M. Eckert-Maksic, H. Lischka, *J. Chem. Phys.* **2006**, *125*, 164323.

[69] M. Barbatti, J. Pittner, M. Pederzoli, U. Werner, R. Mitric, V. Bonacic-Koutecky, H. Lischka, *Chem. Phys.* **2010**, *375*, 26–34.

[70] K. Saita, M. G. D. Nix, D. V. Shalashilin, *Phys. Chem. Chem. Phys.* **2013**, *15*, 16227–16235.

[71] K. R. Yang, X. Xu, J. Zheng, D. G. Truhlar, *Chem. Sci.* **2014**, *5*, 4661–4680.

[72] M. Sapunar, A. Ponzi, S. Chaiwongwattana, M. Malis, A. Prji, P. Decleva, N. Doslic, *Phys. Chem. Chem. Phys.* **2015**, *17*, 19012–19020.

[73] M. Heindl, L. Gonzalez, *Comput. Theor. Chem.* **2019**, *1155*, 38–46.

[74] G. Gregoire, C. Dedonder-Lardeux, C. Jouvet, D. Solgadi, *J. Phys. Chem. A* **2001**, *105*, 5971–5976.

[75] L. Rubio-Lago, G. A. Amaral, A. N. Oldani, J. D. Rodriguez, M. G. Gonzalez, G. A. Pino, L. Banares, *Phys. Chem. Chem. Phys.* **2011**, *13*, 1082–1091.

[76] M. Miyazaki, N. Washio, M. Fujii, *Chem. Phys.* **2018**, *515*, 580–585.

[77] S.-i. Ishiuchi, J. Kamizori, N. Tsuji, M. Sakai, M. Miyazaki, C. Dedonder-Lardeux, C. Jouvet, M. Fujii, *Phys. Chem. Chem. Phys.* **2020**, *22*, 5740–5748.

[78] J. A. Syage, *J. Phys. Chem.* **1995**, *99*, 5772–5786.

[79] O. David, C. Dedonder-Lardeux, C. Jouvet, *Int. Rev. Phys. Chem.* **2002**, *21*, 499–522.

[80] A. L. Sobolewski, W. Domcke, *Chem. Phys. Lett.* **1999**, *315*, 293–298.

[81] A. L. Sobolewski, W. Domcke, *Chem. Phys. Lett.* **2000**, *329*, 130–137.

[82] A. L. Sobolewski, W. Domcke, *J. Phys. Chem. A* **2001**, *105*, 9275–9283.

[83] J. Ehrmaier, D. Picconi, T. N. V. Karsili, W. Domcke, *J. Chem. Phys.* **2017**, *146*, 124304.